Simulation Research on ASF Grid Establishment Methods

Yun Li *, Yu Hua , Bao-Rong Yan , Wei Guo

Posted Date: 27 February 2026

doi: 10.20944/preprints202602.1211.v1

Keywords: enhanced long-rang navigation(eLoran); additional secondary factor (ASF) grid; simulation; the interpolation algorithm

Article

Simulation Research on ASF Grid Establishment Methods

Yun Li *, Yu Hua, Bao-Rong Yan and Wei Guo

The National Time Service Center, Chinese Academy of Sciences, Xi'an 710600, China

* Correspondence: liyun@ntsc.ac.cn; Tel.: 18682911626

Abstract

The ASF grid is one of the important methods for improving the performance of the eLoran system. When an ASF grid is established, users can calculate ASF through the ASF grid database and bilinear interpolation algorithms, thereby obtaining high-precision ASF values. However, establishing an ASF grid is a complex process, involving not only extensive data collection tasks but also the cumbersome processing of the collected data. This paper investigates and analyzes algorithms for establishing ASF grids under different conditions. When the number of test points exceeds the number of grid vertices, grids built using interpolation algorithms—particularly the inverse bilinear interpolation algorithm—perform the best, while those constructed using the Kriging algorithm perform second best, and the inverse distance interpolation algorithm yields the largest errors. When the number of test points is less than the number of grid vertices, grids constructed using the Kriging algorithm perform the best, while the inverse distance interpolation algorithm produces the largest errors. As a result, the inverse bilinear interpolation algorithm is the best choice, when the test points are more than the grid points. The Kriging algorithm is recommended, when the test points are sparse.

Keywords: enhanced long-rang navigation(eLoran); additional secondary factor (ASF) grid; simulation; the interpolation algorithm

1. Introduction

When the eLoran system is selected as the backup system for GNSS systems, countries worldwide are dedicated to research and engineering efforts aimed at improving the accuracy of the eLoran system, to narrow the precision gap between eLoran and GNSS systems. These initiatives include the construction of additional eLoran transmitting stations and the deployment of differential stations across various regions to further enhance the accuracy of time transfer and positioning provided by the eLoran system. As a large-scale radio system, there are transmission errors, signal propagation channel errors, and signal reception errors, among which channel errors represent the most significant unknown component.

Due to the complexity and diversity of terrain, geology, ground cover, altitude, and weather conditions along the signal propagation path, It is difficult to precisely quantify the corresponding parameters. Consequently theoretical calculations of signal propagation path delay deviate significantly from actual conditions, leading to signal propagation path delay errors, which constitute the largest uncertainty within the system's overall error. Within this error, the ASF (Additional Secondary Factor) error represents the predominant component.

Improving the calculation accuracy of ASF is a primary method for enhancing system precision. Initially, various theoretical models are employed to fit real path conditions to further improve ASF prediction accuracy. For example, the research team led by Xi Xiaoli at Xi'an University of Technology has been dedicated to predicting and calculating ASF using different algorithms [1–5], including the parabolic equation, the pulse parabolic equation, FDTD algorithm and so on, which represents the most traditional approach.

 doi:10.20944/preprints202602.1211.v1

Subsequently, the accuracy of ASF is improved by integrating theoretical calculations with actual measurements. For instance, reference stations are established to conduct real-time delay measurements, and the calculated differential corrections are transmitted to users. These users then apply these corrections to refine their own predicted delays, thereby obtaining time components of higher precision [6–8]. In current, this is the universal and mature method for improving ASF accuracy in the eLoran system.

Establishing an ASF grid is also a method to improve the ASF prediction accuracy of the eLoran system. The regional ASF maps is generated based on ASF survey data from this area. Once the ASF grid has been established, users within the region can calculate their ASF values using the ASF values at the grid vertices and a bilinear interpolation algorithm. The methods and procedures adopted for this technical process are relatively mature.

However, building a regional ASF grid database is neither simple nor straightforward. Firstly, it requires data measurements, after which different algorithms must be selected based on the quantity and distribution of the measured data to process the data and construct the ASF grid. For example, engineers in South Korea have used the Universal Kriging algorithm with measured data to generate ASF maps, studying how to overcome the coastline effect of ASF near coastlines by combining measured data and the Universal Kriging algorithm to produce ASF maps [9]. Meanwhile, engineers in the UK and the US have conducted testing at river estuaries and used the interpolation algorithm to construct ASF maps [10].

In this paper, the ASF (Additional Secondary Factor) map generation in various scenarios are simulated with different algorithms under varying quantities of measure points. And the accuracy of the ASF grids generated by these algorithms is analyzed and compared. The performance is first evaluated from the perspective of the grid, followed by an analysis of grid performance from the user's standpoint. Based on this, optimal algorithms are selected for establishing the ASF grid database under different conditions. The study finds that when test points are sufficient, the inverse bilinear interpolation algorithm yields the best grid performance, followed by the Kriging algorithm, while the inverse distance weighting interpolation algorithm exhibits the largest error. When test points are insufficient (i.e., the number of test points is fewer than the number of grid vertices), the inverse bilinear interpolation algorithm cannot be applied. In such cases, the Kriging algorithm and inverse distance weighting interpolation algorithm are employed, with the grid constructed by the Kriging algorithm outperforming that of the inverse distance weighting interpolation algorithm.

2. Materials and Methods

2.1. Inverse Bilinear Interpolation Algorithm

The Inverse Bilinear Interpolation Algorithm is the inverse operation of the Bilinear Interpolation Algorithm. While the Bilinear Interpolation Algorithm determines the attribute values of internal grid points based on known attributes at the four vertices of the grid, the Inverse Bilinear Interpolation Algorithm solves for the attribute values at the grid vertices using known attributes of internal grid points. In this paper, the attribute in question refers to ASF (Additional Secondary Factor) values.

2.1.1. The Bilinear Interpolation Algorithm

The bilinear interpolation algorithm performs linear interpolation separately in the x and y directions, as illustrated in Figure 1. As shown in Figure 1, performing interpolation first in the x-direction and then in the y-direction yields the same result as doing so in the reverse order—the outcome is independent of the sequence of interpolation. The coordinates of the four vertices A, B, C, and D are given as: $A(x_1, y_1)$, $B(x_2, y_1)$, $C(x_1, y_2)$ and $D(x_2, y_2)$, and the corresponding ASF values are C_1, C_2, C_3 and C_4 respectively, So the ASF value at the point to be interpolated is given by Equation (1).

 doi:10.20944/preprints202602.1211.v1

$$ASF = (1-\alpha)[(1-\beta)*C_1 + \beta*C_3] + \alpha[(1-\beta)*C_2 + \beta*C_4], \quad (1)$$

Where $\begin{cases} \alpha = (x - x_i)/(x_{i+1} - x_i) \\ \beta = (y - y_j)/(y_{j+1} - y_j) \end{cases}$ x_i is the longitude, and y_i is the latitude.

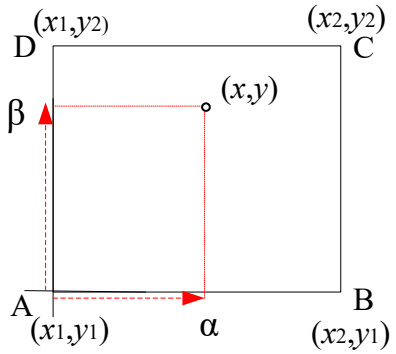

Figure 1. Bilinear Interpolation Algorithm.

2.1.2. Inverse Bilinear Interpolation Algorithm

A single grid cell with 10 test points in it is given as an example for explanation. Using the inverse bilinear interpolation algorithm, the calculation process is shown in Equation (2).

$$\begin{bmatrix} (1-\alpha_1)(1-\beta_1) & \alpha_1(1-\beta_1) & (1-\alpha_1)\beta_1 & \alpha_1\beta_1 \\ (1-\alpha_2)(1-\beta_2) & \alpha_2(1-\beta_2) & (1-\alpha_2)\beta_2 & \alpha_2\beta_2 \\ \cdots & \cdots & \cdots & \cdots \\ (1-\alpha_{10})(1-\beta_{10}) & \alpha_{10}(1-\beta_{10}) & (1-\alpha_{10})\beta_{10} & \alpha_{10}\beta_{10} \end{bmatrix} * \begin{bmatrix} C1 \\ C2 \\ C3 \\ C4 \end{bmatrix} = \begin{bmatrix} ASF_1 \\ ASF_2 \\ \cdots \\ ASF_{10} \end{bmatrix}, \quad (2)$$

The ASF values of the four vertices of the grid are obtained as shown in Equation (3).

$$\begin{bmatrix} C1 \\ C2 \\ C3 \\ C4 \end{bmatrix} = (A'*A)^{-1} * A'* \begin{bmatrix} ASF_1 \\ ASF_2 \\ \cdots \\ ASF_{10} \end{bmatrix}, \quad (3)$$

Where $A = \begin{bmatrix} (1-\alpha_1)(1-\beta_1) & \alpha_1(1-\beta_1) & (1-\alpha_1)\beta_1 & \alpha_1\beta_1 \\ (1-\alpha_2)(1-\beta_2) & \alpha_2(1-\beta_2) & (1-\alpha_2)\beta_2 & \alpha_2\beta_2 \\ \cdots & \cdots & \cdots & \cdots \\ (1-\alpha_{10})(1-\beta_{10}) & \alpha_{10}(1-\beta_{10}) & (1-\alpha_{10})\beta_{10} & \alpha_{10}\beta_{10} \end{bmatrix}$

If there are N grid vertices and M test points within a given region, the ASF values at the N vertices are solved using the ASF values from the M test points. In this case, the coefficient matrix A is an M × N matrix.

2.2. Inverse Distance Weighting Interpolation Algorithm

The attribute value of points are interpolated using a linear weighted combination of the attributes from sample points in the Inverse Distance Weighting (IDW) interpolation algorithm. In this context, the weights are defined as the square of the distance (i.e., distance raised to the power of 2). The calculation formula is shown (4) below.

$$Z^*(x,y) = \sum_{i=1}^{n} \omega_i \cdot Z(x_i, y_i), \quad (4)$$

 doi:10.20944/preprints202602.1211.v1

$$\omega_i = \frac{d_i^{-2}}{\sum_{i=1}^{n} d_i^{-2}}$$

Where

2.3. Kriging Interpolation Algorithm

The Kriging interpolation algorithm is primarily used in geostatistics and was developed to address problems related to ore reserve estimation and error assessment. The fundamental theoretical basis of the Kriging algorithm is the principle that points close in spatial proximity tend to have similar attributes. Therefore, it estimates the attribute values of unknown points by combining the known attributes of sampled points. There are a series of observation points, with the attributes of within a region. The attribute of the point to be interpolated can be expressed by the following formula. It is the most important to determine ω_i the attribute of each known point.

$$z^*(x_0) = \sum_{i=1}^{n} \omega_i z(x_i) \quad (5)$$

,

2.3.1. The Ordinary Kriging

The Ordinary Kriging interpolation algorithm is adopted in this paper. The assumptions of the Ordinary Kriging algorithm are: the spatial attribute z within the region is intrinsically stationary, meaning that for any spatial point (x, y), it has the same expected value C and variance. That is to say, the attribute value at any given point is composed of the regional average C and the local random residual at that point. This relationship can be expressed by the model: ASF values vary continuously and gradually within a homogeneous medium region, this spatial continuity satisfies the intrinsic stationarity assumption required for the Ordinary Kriging method. Of course, in areas such as coastal transition zones or regions with significant topographic relief, where ASF exhibits substantial fluctuations, such scenarios fall outside the scope of this paper.

The variogram characterizes spatial variability by describing the regionalized variation of attributes. Attributes at locations that are closer together tend to be more highly correlated, while those farther apart are less correlated. The estimated value at the unsampled location is then given by the Formula (6)

$$ASF^*(x_0) = \sum_{i=1}^{n} \omega_i ASF(x_i) \quad (6)$$

,

2.3.2. The Variogram Modeling for Ordinary Kriging

The Variogram modeling for Ordinary Kriging is a core step, used to quantify the spatial autocorrelation structure of the data. The variogram describes how the variance of the difference between values at two points in space changes with their separation distance (and direction). Its basic definition is:

$$\gamma(ij) = \frac{1}{2} E\left[(Z(i) - Z(j))^2 \right] \quad (7)$$

,

Where $\gamma(ij)$ is the variogram value of the i and j pont, $Z(i)$ and $Z(j)$ is the observed value at the i and j point. and h_{ij} is the distance from the i point and j point.

Based on the measured data, first calculate the distance the lag distance h_{ij}, and compute their attribute difference γ_{ij}. This process generates multiple data pairs of lag distance and attribute difference, denoted as(h_{ij}, γ_{ij}). Following the principles of variogram analysis, an appropriate

 doi:10.20944/preprints202602.1211.v1

theoretical variogram model is selected and fitted to the data. This yields a variogram function specifically tailored to the application scenario. Commonly used theoretical variogram models include the Gaussian, exponential, spherical models, and show in the Figure 2 and Formula (8). The green straight line is the sill and the red straight line is the lag distance. In the figure, the sill is 1,and the lag distance is 15 in figure (a), and the sill is about 0.9 and the lag distance is 6 in exponential, In figure (c), the sill is 1 and the lag distance is about 8.

$$\gamma(h) = \begin{cases} C\left(1-e^{-\left(\frac{h}{a}\right)^2}\right), & Gaussian \\ C\left(1-e^{\left(-\frac{h}{a}\right)}\right), & \text{exponential} \\ C\left(\frac{3h}{2a}-\frac{1}{2}\left(\frac{h}{a}\right)^3\right), & \text{spherical} \end{cases}, \tag{8}$$

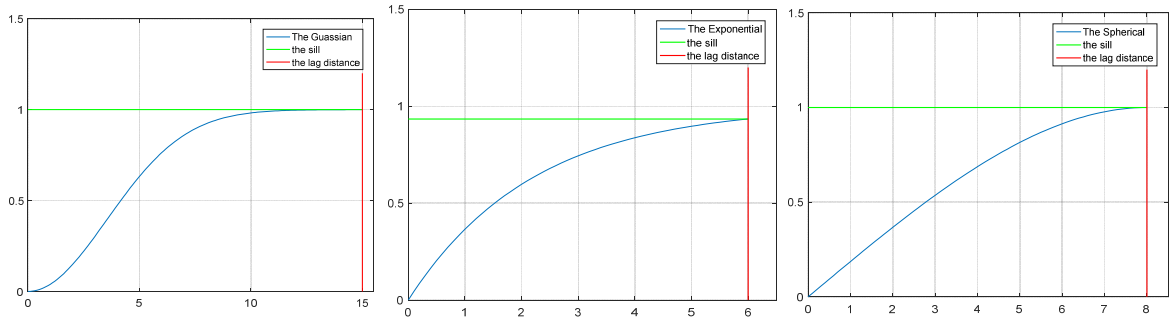

(a) (b) (c)

Figure 2. The Theoretical Variogram Models,(a) the guassian model (b) the exponential model and(c) the spherical mode.

Once the experimental semivariogram is obtained, the relationship between spatial location and correlation is determined. Substituting the positional relationship between the point to be estimated and the known points into the experimental semivariogram yields the correlation between the target point and the known points, which constitutes the matrix on the right-hand side of the equation.The weights for all known sample points are computed from the experimental variogram, then the estimated value at the unsampled location is calculated in Formula (9).

$$\begin{bmatrix} \omega_1 \\ \omega_2 \\ \cdots \\ \omega_n \\ \lambda \end{bmatrix} = \begin{bmatrix} 0 & \gamma_{12} & \gamma_{13} & \cdots & \gamma_{1n} & 1 \\ \gamma_{21} & 0 & \gamma_{23} & \cdots & \gamma_{2n} & 1 \\ \cdots & \cdots & \cdots & \cdots & \cdots & \cdots \\ \gamma_{n1} & \gamma_{n2} & \gamma_{n3} & \cdots & 0 & 1 \\ 1 & 1 & \cdots & \cdots & 1 & 0 \end{bmatrix}^{-1} \begin{bmatrix} \gamma_{01} \\ \gamma_{02} \\ \cdots \\ \gamma_{0n} \\ 1 \end{bmatrix}, \tag{9}$$

3. Result

Three algorithms—Inverse Bilinear Interpolation, Inverse Distance Weighting(IDW), and Kriging algorithms—are employed in the paper. Simulations are conducted in a progressive manner, starting from a single grid cell, then to four grid cells, and finally to multiple grid cells.

 doi:10.20944/preprints202602.1211.v1

3.1. Single-Grid Simulation

Within a single grid cell at a 0.02° interval, five test points in green are randomly distributed as illustrated in Figure 3. There are two user points in blue. This simulation scenario in the following context is referred to as Scenario 1.

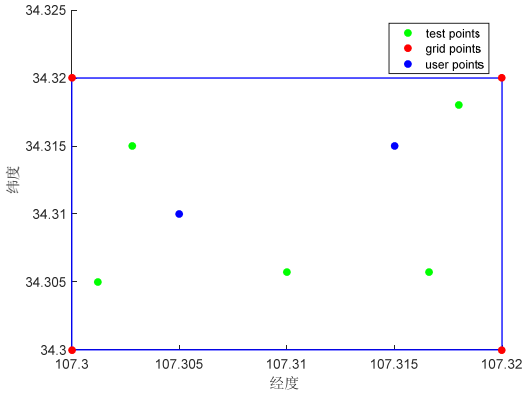

Figure 3. Distribution of Grids Test Points and users points.

3.1.1. Grid Vertex ASF

The inverse bilinear interpolation algorithm, Kriging algorithm, and inverse distance weighting interpolation algorithm are employed to determine the ASF values at grid vertices. In the kriging algorithm, three models are used to simulate the semivariogram function. The resulting parameters for each model are shown in the Table 1 below. The Gaussian model has the smallest error.Ultimately, we selected the Gaussian model for use.

Table 1. RSS value of the three variogram models for ordinary kriging.

Model	Sill/μs²	Range/km	RSS/μs²
Gaussian model	0.0024	2.8	1.056×10^{-6}
Exponential model	0.013	12	3.782×10^{-6}
Spherical model	0.0049	3.6	3.125×10^{-6}

As can be seen from the interpolation result curve in Figure 4(a), the result of the Inverse Bilinear Interpolation algorithm almost coincides with the theoretical value, followed by the Kriging algorithm. whereas the result of the Inverse Distance Weighting (IDW) algorithm shows a significant deviation from it. The error curve in Figure 4(b) reveals that the error of the Inverse Bilinear Interpolation algorithm at the four points is nearly zero, while the error of the Kriging is less than 2ns, and the error of the Inverse Distance Weighting (IDW) algorithm remains within 5 ns. the Inverse Bilinear Interpolation algorithm yields ASF values at the grid vertices that are clearly superior to those produced by the Kriging algorithm, and the Kriging algorithm outperforms the IDW algorithm.

 doi:10.20944/preprints202602.1211.v1

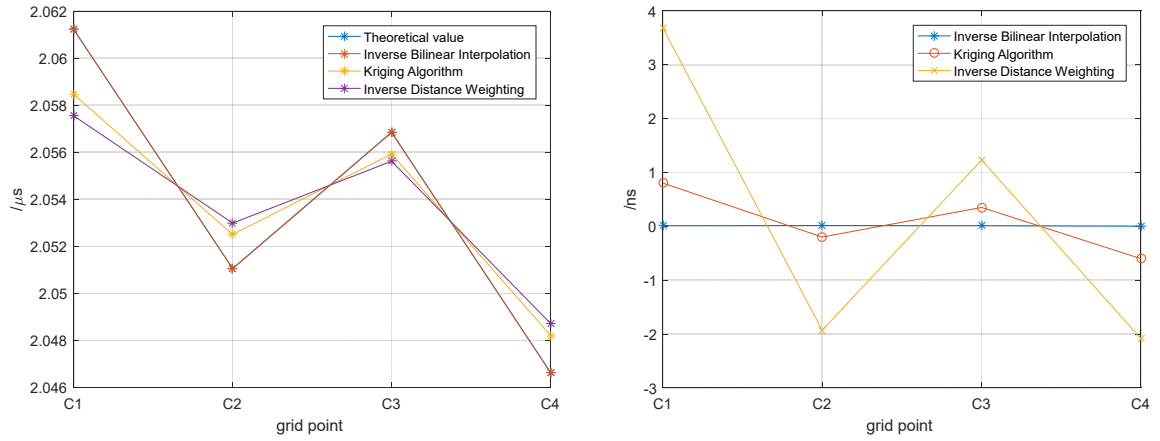

(**a**) (**b**)

Figure 4. Results of the interpolation algorithm, a) Interpolation results at grid vertices, b) Interpolation error at grid vertices.

3.1.2. The ASF of Users Points

The user points, denoted by blue dots, are also included in the Figure 3 The ASF value at a user point is solved using a pre-established ASF grid and bilinear interpolation. The obtained results are presented in Table 1 below. For ease of identification, the mesh obtained using Inverse Bilinear Interpolation algorithm is referred to as the IBI-grid. The mesh obtained using Kriging Interpolation algorithm is referred to as the Kriging-grid. The mesh obtained using IDW algorithm is referred to as the IDW-grid.

Table 2. ASF of User Points.

Longitude/°	Latitude/°	Theory/μs	IBI-grid/μs	Kriging-grid/μs	IDW-grid/μs
107.3050	34.3100	2.0565	2.0563	2.0528	2.0492
107.3150	34.3150	2.0503	2.0509	2.0480	2.0584

In Figure 5 the variance of the result obtained using the grid built with Inverse Bilinear Interpolation is nearly zero, while the variance for the result based on the grid built with kriging is less than 5ns. while the variance for the result based on the grid built with IDW is about 10ns. Therefore, the grid constructed using the Inverse Bilinear Interpolation algorithm yields higher accuracy than the one built with the Kriging, meanwhile, the grid with Kriging outperforms the Inverse Distance Weighting (IDW) algorithm. Consequently, the Inverse Bilinear Interpolation algorithm outperforms the Kriging Algorithm, while the Kriging Algorithm is superior to the IDW Algorithm.

 doi:10.20944/preprints202602.1211.v1

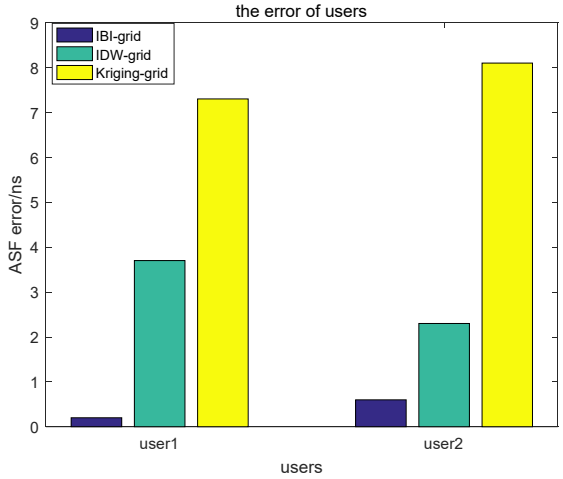

Figure 5. the accuracy of individual test points.

3.2. Four-Grid Simulation

Further simulation analysis of the interpolation algorithms was conducted in a four-grid environment. This simulation scenario in the following context is referred to as Scenario 2.

3.2.1. Grid Vertex ASF

The grid spacing is 0.02°, and the grid partitioning along with the distribution of test points are illustrated in Figure 6, and the magenta points are user points. Three algorithms were employed for the calculations: Inverse Bilinear Interpolation, Kriging algorithms, Inverse Distance Weighting (IDW).

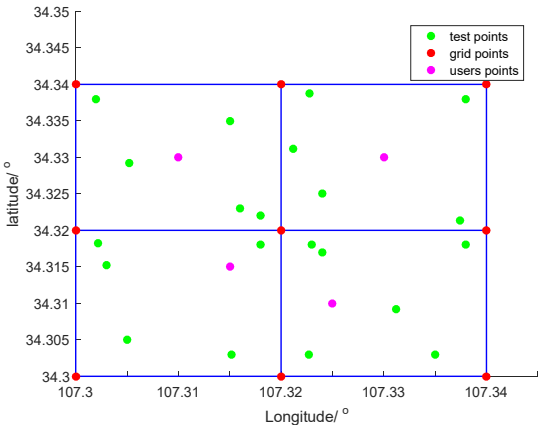

Figure 6. Distribution of Test Points and Grids.

The gaussian model, the exponential model and the spherical model were compared and analyzed in Figure 7 and Table 3 The RSS of the Gaussian is 1.386×10^{-6} and the sill value is 0.0076 μs^2 , and the corresponding range is approximately 5 km. The error of the exponential mode is 4.122×10^{-6}, the sill is 0.027 μs^2 ,and the lag range is 44km.The error of spherical model is 3.775×10^{-6},the sill is 0.0082 μs^2 ,the lag range is 6.4km.the Gaussian model is smallest. Consequently, the Gaussian model was ultimately selected as the semivariogram function.

 doi:10.20944/preprints202602.1211.v1

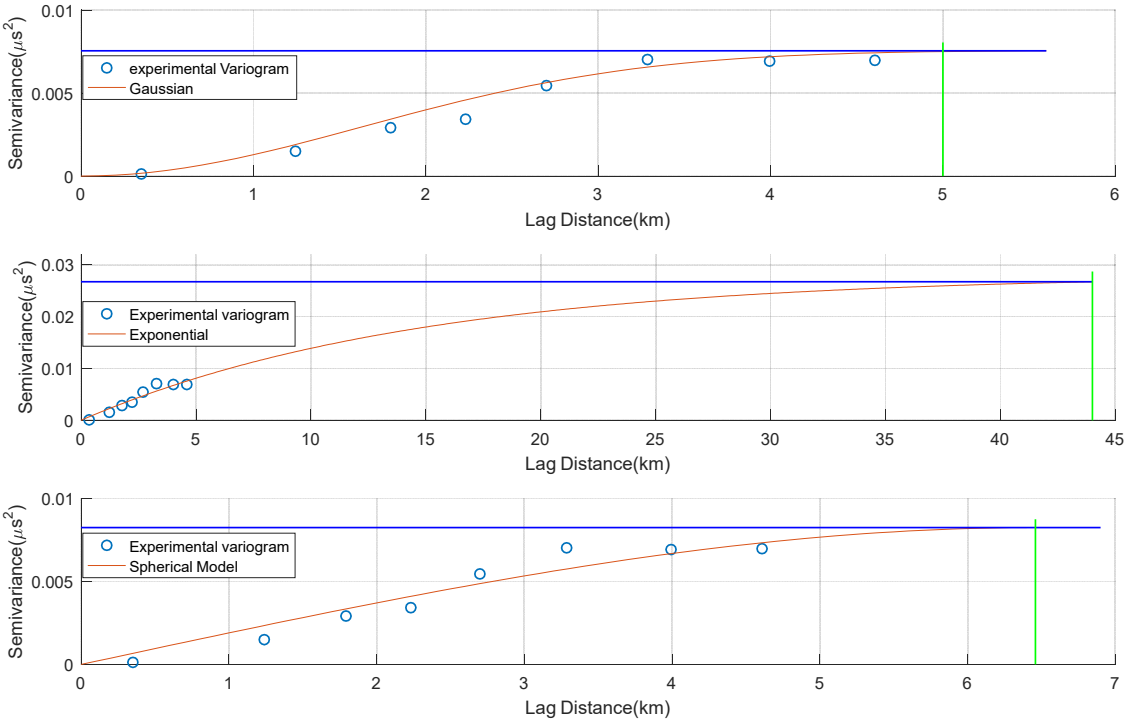

Figure 7. Variogram Graph.

Table 3. RSS value of the three variogram models for ordinary kriging.

Model	Sill/μs²	Range/km	RSS/μs²
Gaussian model	0.0076	5	1.386×10^{-6}
Exponential model	0.027	44	4.122×10^{-6}
Spherical model	0.0082	6.4	3.775×10^{-6}

The computational results of the three algorithms are shown in Figure 8 below. The inverse bilinear interpolation algorithm yields result closest to the theoretical values, followed by the Kriging interpolation algorithm, while the ASF calculated by the inverse distance weighting (IDW) interpolation algorithm exhibit significant deviations from the theoretical values. As can be seen from Figure 8, the error of the inverse bilinear interpolation algorithm is nearly zero, the error of the Kriging interpolation algorithm is less than 5 ns, and the error of the IDW interpolation algorithm is less than 10 ns. Overall, the inverse bilinear interpolation algorithm achieves the highest accuracy in solving the ASF grid, followed by the Kriging algorithm, while the IDW method yields the largest error in the ASF grid calculations.

 doi:10.20944/preprints202602.1211.v1

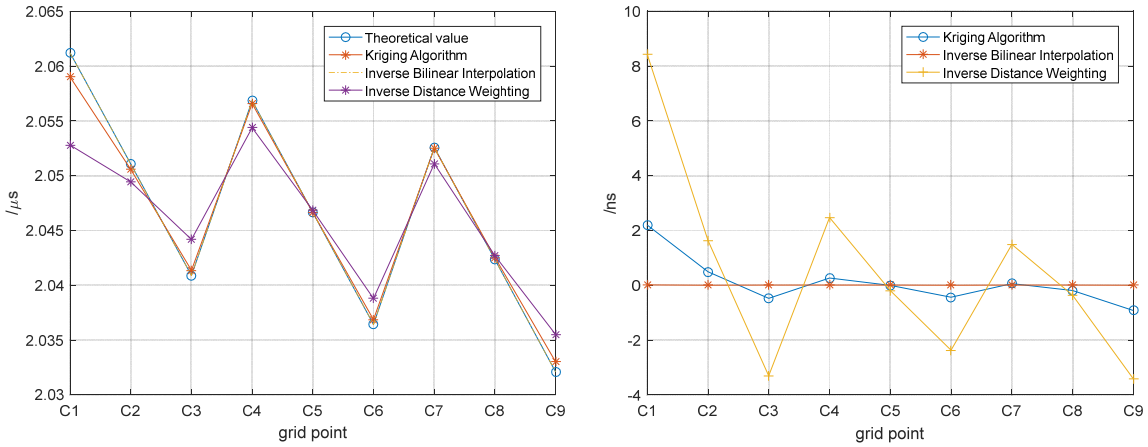

(**a**) (**b**)

Figure 8. The computational results of various algorithms(a)the ASF of the grid point(b)the error for the grid point ASF.

3.2.2. The ASF of Users Points

The users point is indicated in magenta in Fiugre.5, We obtained the mesh using three algorithms. The ASF at the user point was calculated using three different meshes and the bilinear interpolation algorithm.

The result of user ASF are shown in Table 4 and the error Figure 9. The three results were compared with the theoretical values, and the errors between them are shown in Figure 14. Under this simulation environment, the error of the user's ASF calculated using the IBI-grid is within 10 ns, the error of the user's ASF calculated us-ing the Kriging-grid is within 15 ns, and the error of the user's ASF calculated using the IDW-grid is within 20 ns. The user error calculated using the IBI-grid is the smallest, the error calculated using the IDW-grid is the largest, and the error calculated using the Kriging-grid falls in between. This also demonstrates that Inverse Bilinear Interpolation algorithm outperforms Inverse Distance Weighting algorithm, while Kriging Interpolation algorithm's performance lies between that of Inverse Bilinear Interpolation algorithm and the Inverse Distance Weighting algorithm.

Table 4. ASF Values at User Points.

Longitude/°	Latitude/°	Theoretical value/μs	IBI-grid/μs	Kriging-grid/μs	IDW-grid/μs
107.3150	34.3150	2.0503	2.0543	2.0448	2.0621
107.3250	34.3100	2.0463	2.0413	2.0572	2.0345
107.3100	34.3300	2.0496	2.0526	2.0585	2.0578
107.3300	34.3300	2.0394	2.0374	2.0310	2.0440

Preprints.org (www.preprints.org) | NOT PEER-REVIEWED | Posted: 27 February 2026 doi:10.20944/preprints202602.1211.v1

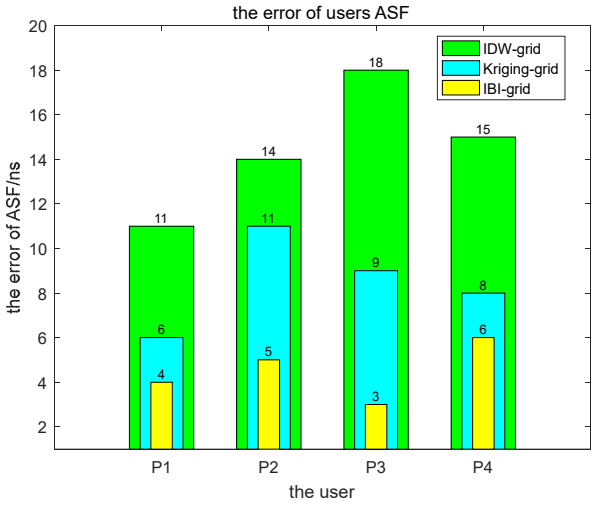

Figure 9. the error os users ASF.

3.3. Multiple-Grid Simulation

3.3.1. Grid Vertex ASF

The simulation environment is shown in Figure 10 below, with a grid spacing of 0.02. The positions of the test points and grid points are as illustrated: the green dots represent test points, and the red dots represent grid vertices, which are enclosed within the test points. This simulation scenario in the following context is referred to as Scenario 3.The number of unknowns is greater than the number of test points, making system of equations unsolvable. Therefore, the inverse bilinear interpolation algorithm cannot be applied. In this study, the Kriging algorithm and the inverse distance weighting (IDW) algorithm are used to estimate the ASF values at the grid vertices.

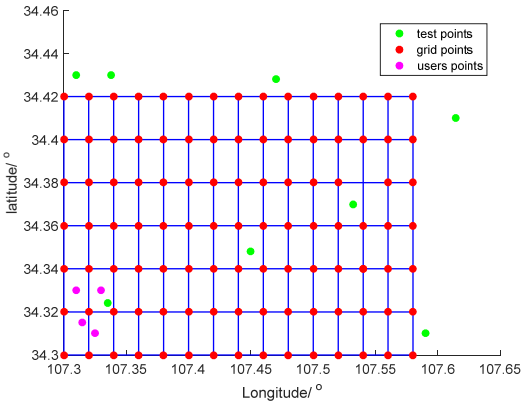

Figure 10. Distribution of Test Points and Grid Points.

In the kriging algorithm, three theoretical variograms is used. The sill is 0.01 μs^2, and the lag range is 23km, The Rss is 0.0003969 μs^2 for the spherical model. The sill is 0.01 μs^2, and the lag range is 33km, The Rss is 0.0006451 μs^2 for the exponential model. The sill is 0.01 μs^2, and the lag range is 18km, The Rss is 0.0002479 μs^2 for the gaussian model. The error of the gaussian is the minimum, so it is selected to analysis the measure data.

 doi:10.20944/preprints202602.1211.v1

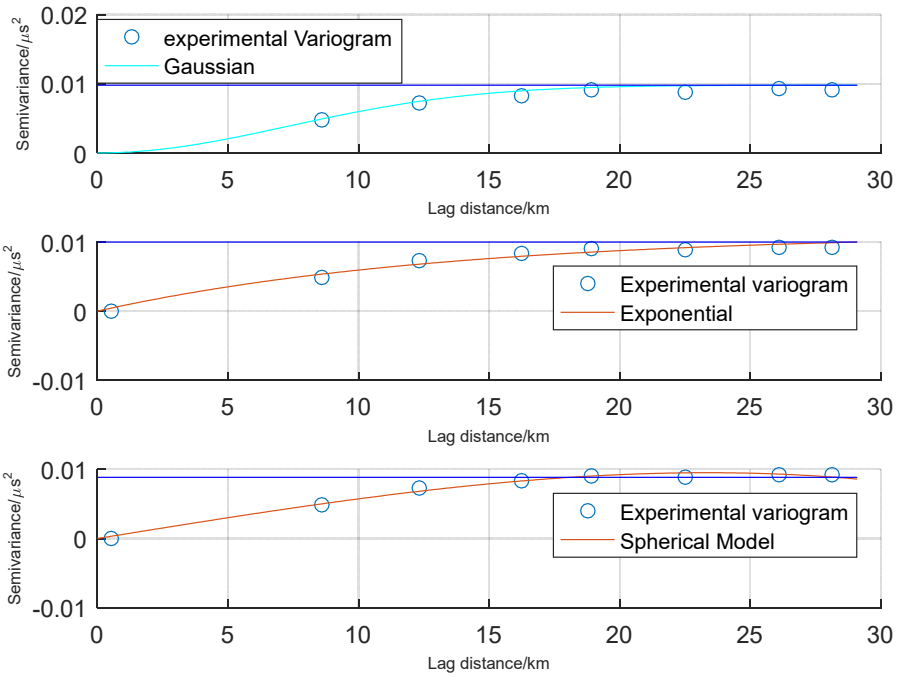

Figure 11. Experimental variogram and three theoretical variograms.

Table 5. RSS value of the three variogram models for ordinary kriging.

Model	Sill/μs²	Range/km	RSS/μs²
Gaussian model	0.01	18	0.0002479
Exponential model	0.01	33	0.0006451
Spherical model	0.01	23	0.0003969

The ASF values obtained through these two methods in the simulation are presented in Figure 12. The error curves obtained from the simulation are shown in Figure 13. From the error curves, it can be observed that the errors at all grid vertices are within 50 ns. The error of the Kriging algorithm is around 20 ns, while the error of the IDW algorithm is within 50 ns. This indicates that the Kriging algorithm achieves higher accuracy than the IDW algorithm.

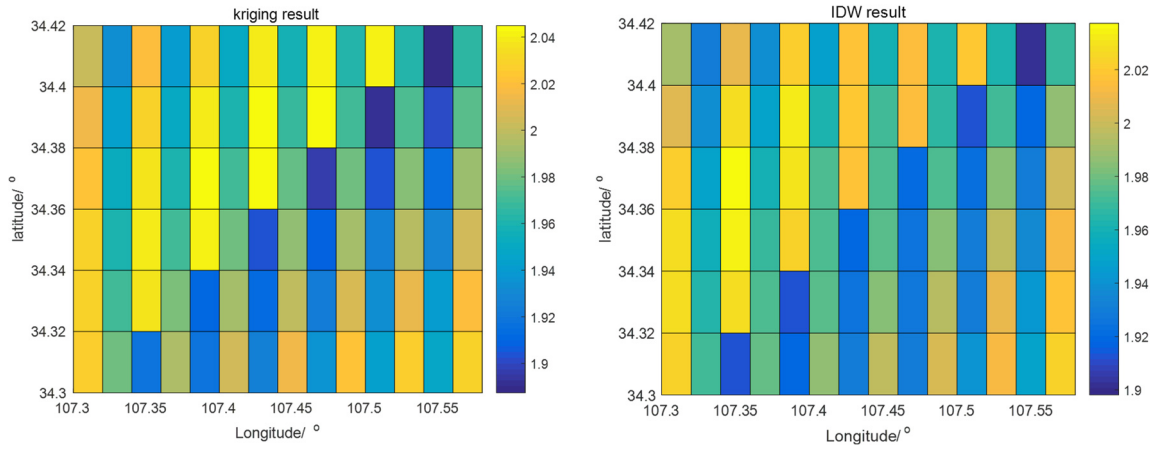

(**a**) (**b**)

Figure 12. ASF at grid vertices, (a) Results of the IDW Algorithm, (b) Results of the Kriging.

 doi:10.20944/preprints202602.1211.v1

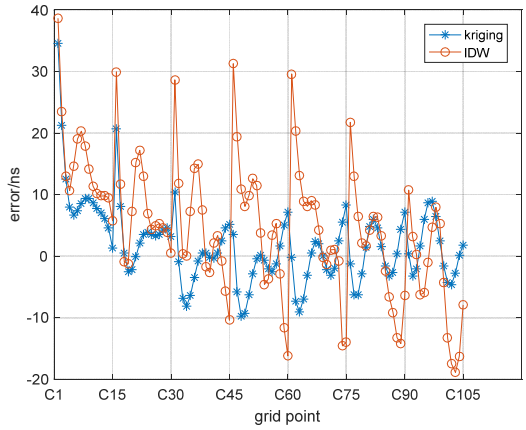

Figure 13. Error distribution at grid vertices.

3.3.2. The ASF of Users Points

The user points are represented by a magenta dot in the Figure 10. For ease of analysis and comparison, the geographical locations of these user points are the same as those in Section 4.2. The result of the users is shown in Table 6. The error of the users ASF is shown in Figure 14. The errors of users ASF in kriging-grid are all with in 50ns, and the errors of users ASF in IDW-grid are all greater than 50 and less than 100. In the perspective of ASF accuracy, the mesh constructed using the Kriging algorithm is superior to that generated by the IDW algorithm. Although the mesh constructed using the IDW algorithm exhibits larger errors, it still outperforms a threshold of 100 ns.

Table 6. ASF of User Points.

Longitude/°	Latitude/°	theoretical value/μs	Kriging-grid/μs	IDW-grid/μs
107.3150	34.3150	2.0503	2.0284	2.1094
107.3250	34.3100	2.0463	2.0734	2.1011
107.3100	34.3300	2.0496	2.0676	1.9884
107.3300	34.3300	2.0394	2.0166	2.0855

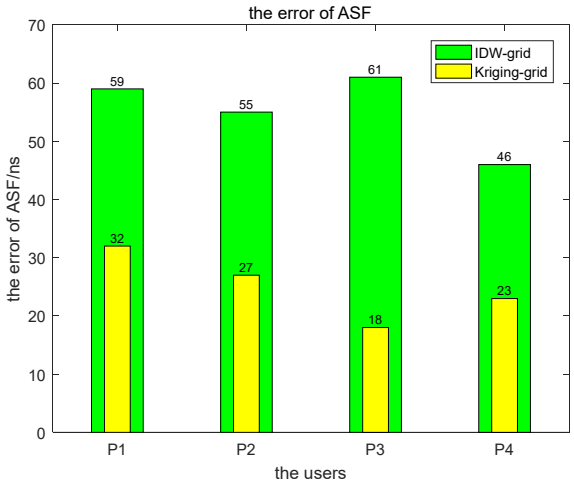

Figure 14. the error os users ASF.

 doi:10.20944/preprints202602.1211.v1

4. Discussion

In this section, the ASF values at grid vertices and user points across the three scenarios are compared. Since Scenario 1 involves only a single grid and is relatively straightforward, it is not included in the detailed comparison. Because Scenario 2 and Scenario 3 share the same set of user points, a thorough comparison is conducted between them. The focus here is primarily on comparing the ASF values of the identical grid vertices and user points established in both Scenario 2 and Scenario 3.

4.1. Compare the Grids ASF Established in Scenario 2 and Scenario 3

In section3, The ASF grids established by different algorithms under the same scenario are compared. Here, we analyze the grids established by the same algorithm under different scenarios as shown in the Figure 15, when using the Kriging interpolation algorithm, the error is less than 5 ns in Scenario 2, and less than 20 ns in Scenario 3. For the inverse distance interpolation algorithm, the error does not exceed 20 ns in Scenario 2, and does not exceed 10 ns in Scenario 3. Regardless of which algorithm is used, the grid established in Scenario 2 outperforms that in Scenario 3, indicating that more testing points result in higher precision of the ASF values at the grid vertices.

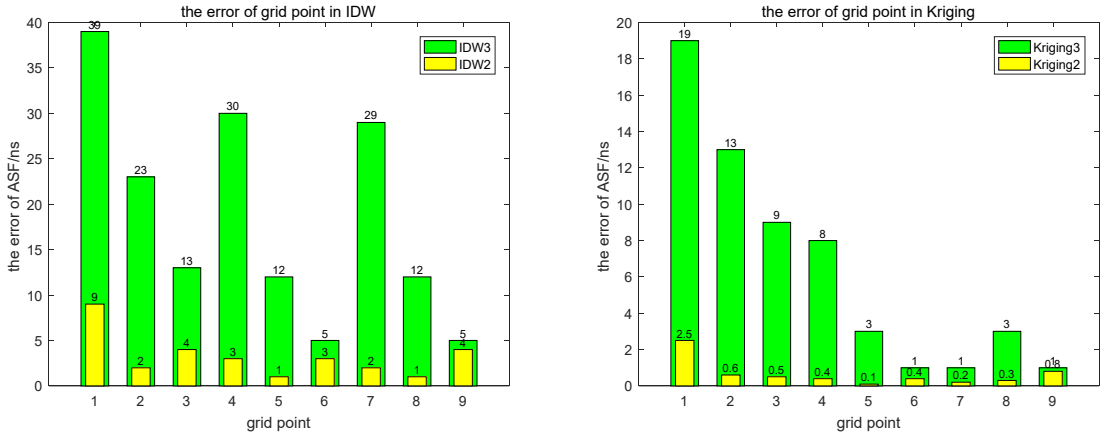

(**a**) (**b**)

Figure 15. the error of the grid point a)the grid build by the IDW in Scenario 2 and Scenario 3. b) the grid build by the IDW in Scenario 2 and Scenario 3.

4.2. Compare the ASF of User Points Between Scenario 2 and Scenario 3

In the analysis of the previous section, it was concluded that the accuracy of the grid established in Scenario 2 is superior to that in Scenario 3. The ASF for users was calculated using the grids established from Scenario 2 and Scenario 3, respectively, and the results are shown in Figure 16. For point P1, the ASF at user point P1 was calculated using the grid established by the Kriging algorithm. The error in the result for Scenario 2 is 6 ns, while that for Scenario 3 is 32 ns, indicating that the result from Scenario 2 outperforms that from Scenario 3. When calculating the ASF at user point P1 using the grid generated by the inverse distance interpolation algorithm, the error in Scenario 2 is 11 ns, while in Scenario 3 it is 59 ns. This indicates that the accuracy of Scenario 2 is superior to that of Scenario 3. Comparing the calculation results for each point using the same algorithm in both scenarios, it is concluded that the results from Scenario 2 are superior to those from Scenario 3.

 doi:10.20944/preprints202602.1211.v1

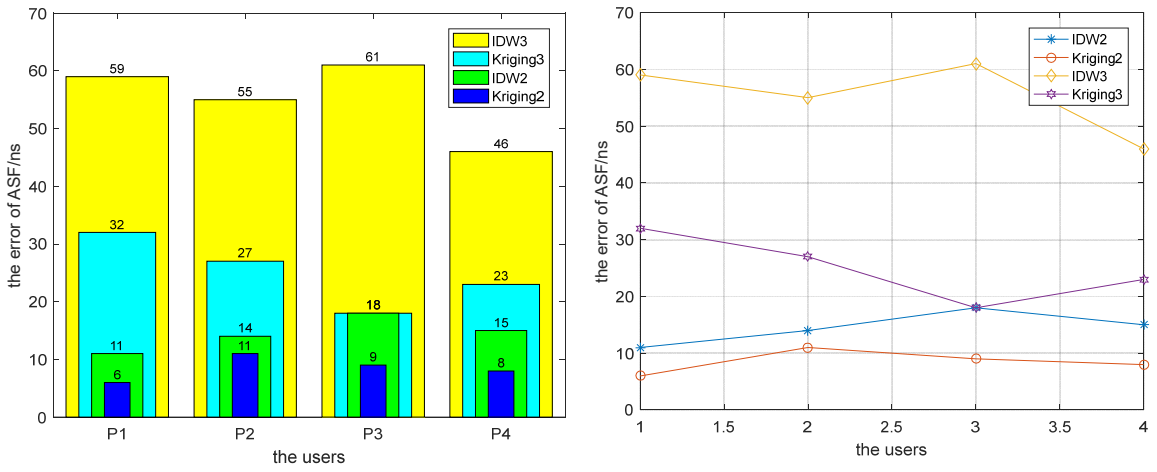

(**a**) (**b**)

Figure 16. the error os users ASF a) User ASF Error Bar Chart,b) User ASF Error Curve Chart.

5. Conclusions

Establishing an ASF grid is an important method for improving the accuracy of the eLoran system, but the process is complex and the methodology is cumbersome.it has been found that when the number of test points in an area exceeds the number of grid vertices, the inverse bilinear interpolation algorithm yields the highest grid accuracy, within 5ns error in 0.02 grid for users, followed by the Kriging interpolation algorithm, while the IDW (Inverse Distance Weighting) interpolation algorithm exhibits the largest error. When the number of test points is smaller than the number of grid vertices, the inverse bilinear interpolation algorithm becomes unusable. In such cases, the Kriging algorithm and the IDW inverse distance weighting algorithm can be employed to construct the grid, with the Kriging interpolation algorithm providing higher grid accuracy, about 30ns error in 0.02 grid.

References

1. D. D. Wang, X. L. Xi, Y. R. Pu, J. F. Liu, and L. L. Zhou, “Parabolic equation method for loran-C ASF prediction over irregular terrain,” IEEE Antennas Wireless Propag. Lett., vol. 15, pp. 734–737, 2016.
2. D.-D. Wang, X.-L. Xi, L.-L. Zhou, Y.-R. Pu, and J.-S. Zhang, “Pulse parabolic equation method for loran-C ASF prediction over irregular terrain,” IEEE Antennas Wireless Propag. Lett., vol. 17, no. 1, pp. 168–171,Jan. 2018.
3. X. L. Xi, L. L. Zhou, J. S. Zhang, and J. F. Liu, “Combined IE-FDTD algorithm forlong-range Loran-Cground-wave propagation,” IEEE Trans.Antennas Propag., vol. 60, no. 8, pp. 3802–3808, Aug. 2012.
4. Dan-Dan Wang, Yu-Rong Pu, Xiao-Li Xi, Li-Li Zhou,” Hybrid FDTD–PE method for Loran-C ASF prediction with near-source complex topography” IET Microw. Antennas Propag., 2020, Vol. 14 Iss. 2, pp. 171-176
5. Li-Li Wang, Zi-Chen Liang, Yu-Rong Pu, and Xiao-Li Xi,” Method for Loran-C Additional Secondary Factor Correction Based on Neural Network and Transfer Learning” IEEE ANTENNAS AND WIRELESS PROPAGATION LETTERS, VOL. 21, NO. 2, FEBRUARY 2022,pp:332-336.
6. Yun Li, Yu Hua, Bao-rong Yan, Wei Guo Experimental Study on a Modifed Method for Propagation Delay of Long Wave Signal, IEEE Antennas and Wireless Propagation Letters Vol:18, Issue:9 P 1716-1720 2019. (SCI, IF 3.448)
7. Yun Li, Yu Hua, Baorong Yan, Wei Guo,” Research on the eLoran Differential Timing Method”, Sensors 2020, 20, 6518
8. Chaozhong Yang, Xiaohang Guo Shifeng Li, and Zhaopeng Hu, ”Design and Performance Evaluation of eLoran Monitoring System”, Appl. Sci. 2024, 14, 7350

 doi:10.20944/preprints202602.1211.v1

9. Pyo-Woong Son, Joon Hyo Rhee, Jaehui Hwang, and Jiwon Seo, "Universal Kriging for Loran ASF Map Generation", IEEE Transactions on Aerospace and Electronic Systems,
10. Song, JunwooSon, Pyo-Woong,' Path-Based Correlation Analysis of Meteorological Factors and eLoran Signal Delay Variations',arXiv,
11. Jianchen Di, JiangningXu,Jun Fu, Bao Li and Miao Wu, Study on the regional ASF prediction method based on the ordinary kriging interpolation, Phys. Scr. 99 (2024) 015026
12. Hargreaves, C., ASF quality assurance for Loran, Proc. Conf. IEEE-ION PLNS, doi: 10.1109 / LANS.2012.6236972, p1169-1174,2012
13. W. J. Gregory, LORAN: Creating a viable backup for GPS [D], University of Rhode Island,2005.
14. Durk van Willigen, et al. eDLoran: The Next-Gen LORAN[J]. GPS World. 25(7) pp. 36-40, 2014.
15. W. J. Gregory, et al. A Procedure for Creating Optimal ASF Grids for Harbor Entrance & Approach ION GNSS 19th.